Thermo-visco mechanical behavior of glass fiber reinforced thermoplastic composite

Josephine Faddoul, Pierre Rahme, Dominique Guines, Lionel Leotoing

Thermo-visco Mechanical Behavior of Glass Fiber Reinforced Thermoplastic Composite

Journal of Composite Materials
XX(X):1–11

DOI: 10.1177/ToBeAssigned
www.sagepub.com/
SAGE

Josephine Faddoul[1,2], Pierre Rahme[2,3], Dominique Guines[1] and Lionel Leotoing[1]

Abstract

Thermoplastic composite materials are being increasingly used in many domains, such as automotive, marine and aeronautics. This growing interest is due to the relatively good mechanical properties and the recycle-ability of these materials. In various heat assisted forming technologies, thermoplastic composites may be subjected to severe conditions such as high temperatures, complex strain paths and potentially significant strain rates. This is expected to highly influence the overall behavior of these materials and make the characterization of their mechanical behavior more complicated. In this paper, the mechanical behavior of discontinuous glass fiber reinforced polypropylene composite is investigated at temperatures going from room temperature (RT) to 120°C and strain rates ranging from quasi-static conditions to 10 s^{-1} by means of uniaxial tensile tests. The effect of material orientation is also investigated at RT and quasi-static strain rate of 0.001 s^{-1} pointing out a clear anisotropic behavior. The tensile properties including Young's modulus E, ultimate tensile strength σ_{ult} and strain at failure ε_f are determined based on the Standard ISO-527 reporting an obvious sensitivity of the material to temperature and strain rate. Based on literature review, the phenomenological isotropic constitutive model of G'Sell and Jonas, originally designed for unreinforced semi-crystalline polymers, is selected to describe the mechanical behavior of the studied material. A modification of the original constitutive equation is proposed for a better representation of the overall behavior of the material at different temperature and strain rate conditions. Finally, the validity of this phenomenological law calibrated by means of the uniaxial tests, is evaluated for an equi-biaxial loading state close to that encountered by the material during heat assisted sheet forming process. The significant disagreement highlighted between numerical and experimental results proved that the uniaxial tensile tests are not sufficient to characterize the behavior of the material when a complex loading condition is imposed.

Keywords

Glass fiber reinforced thermoplastics, Strain rate, Temperature, Mechanical characterization, Heat assisted forming.

Introduction

Composite materials are now widely used in many fields, such as aeronautics, marine and automotive. This is mainly due to the relatively high strength/weight ratio that these materials can offer[1]. There exist several types of composites in which the structure can be composed with different combinations of reinforcement/matrix. Constituents should be wisely selected in order to fulfill the requirements of the intended application as well as the product lifetime, complexity of shape, costs...[2]

More particularly, thermoplastic composites exhibit good mechanical properties as well as recycle-ability. This makes them an eco-friendly alternative to other plastics and metals[3].

Although the use of thermoplastic composites can be advantageous, their sensitivity to temperature and strain rates complicates the study of their mechanical behavior[4]. Such complex conditions can be encountered by the material during heat assisted forming such as hot stamping[5,6] and more particularly for heat assisted incremental sheet forming, already tested for metal sheets but relatively new for thermoplastics. The latter is drawing considerable interests and significant progress has been made recently[7]. The sensitivity of the matrix to severe conditions of temperature and strain rates is expected to be a significant part of the overall mechanical behavior of a fiber reinforced thermoplastic polymer[8,9]. Atmani et al.[9] performed an experimental and numerical study to describe the behavior of an unreinforced thermoplastic polymer (high impact polystyrene HIPS) during plug-assisted thermoforming. In the experimental part of their study, they investigated the elastic properties by performing uniaxial tensile tests at different temperatures, from 80°C to 140°C, and at three different strain rates: $0.0167s^{-1}$, $0.033s^{-1}$, and $0.167s^{-1}$. They noticed that the elastic modulus and the yield strength increased by 67% and 50%, respectively, as the strain rate increased by a factor of 10. Moreover, a temperature

[1]Univ Rennes, INSA Rennes, LGCGM (Laboratoire de Génie Civil et Génie Mécanique) - EA 3913, F-35000, Rennes, France
[2]Faculty of Engineering, Mechanical Engineering Department, Lebanese University, Lebanon
[3]Department of Industrial and Mechanical Engineering, Lebanese American University, Lebanon

Corresponding author:
Josephine Faddoul, INSA-LGCGM-EA3913, 20 Av. des Buttes de Coësmes , CS 70839, 35708 Rennes Cedex 7, France.
Email: josephine.faddoul@insa-rennes.fr

increment of 20°C at the lowest strain rate, caused a decrease in the values of Young's modulus and yield strength by 67% and 54%, respectively. Furthermore, Wang et al.[10], studied the effect of temperature (ranging from 21°C to 100°C) and strain rate (0.05 min^{-1}, 0.5 min^{-1}, 5 min^{-1}) on the mechanical behavior of short glass fiber reinforced polyamide-6. They concluded that increasing the strain rate by a factor of 100 at a temperature of 21°C, induces an increase of 16% and 18% for both Young's modulus and tensile strength, respectively. Whereas, an elevation of temperature from 21°C to 100°C causes a decrease of 75% in Young's modulus and 43% in the tensile strength. Duan et al.[11], investigated the effect of uniaxial strain rate on the mechanical properties of glass fiber reinforced polypropylene at RT. They showed that increasing the strain rate from $0.001s^{-1}$ to $50s^{-1}$ increases the ultimate tensile strength by 84% while having a negligible effect on Young's modulus. Similarly, Cui et al.[12], studied the tensile behavior of long glass fiber reinforced polypropylene at room temperature at a strain rate ranging between $0.001s^{-1}$ and $400s^{-1}$. Results showed that the ultimate strength, fracture strain, and Young's modulus increase by increasing the strain rate. The effect of strain rate on the mechanical behavior was also studied for the case of hybrid composites, i.e. reinforced with natural and synthetic fibers. Basrani et al.[13] investigated the influence of strain rate on a composite reinforced with four different natural fibers in addition to top and bottom layer of glass fibers. It was found that for strain rates ranging from 0.00022 s^{-1} to 0.0888 s^{-1}, the tensile strength of the composite increased by 8% with the increase of the deformation rate.

On the other hand, several studies have been carried out on polymers as well as their corresponding composites to model their mechanical behavior specifically for thermoforming applications. Mooney-Rivlin's model[14] is an example of hyperelastic models that can predict the stress flow of polymeric materials. Gong et al.[15] developed an anisotropic hyperelastic constitutive model to predict the large deformation behavior of woven prepregs during thermo-forming process. Pham et al.[16] predicted the strain rate and temperature dependent stretching behavior of a thermoplastic polymer (polyethylene therephtalate PET) using a visco-hyperelastic model based on Mooney-Rivlin's model. They performed biaxial stretching tests using the "Bruckner stretcher" machine. The model parameters were identified using non-linear curve fitting of biaxial results in MATLAB, based on the Levenberg-Marquardt algorithm. Additionally, Guzman et al.[17] developed a non-linear visco-hyperelastic model based on the generalisation of the Maxwell's rheological model. The objective is to model the forming of pre-impregnated thermoplastic composites. Also, Peng et al.[18] proposed a non-linear thermo-viscoelastic constitutive model, used in thermoforming simulation of a car interior part, to describe the strain rate and temperature dependent behavior of a polypropylene wood composite. The Cowper-Symonds viscoplastic model, originally designed for metals, was applied in some studies to model the behavior of fiber reinforced polymers[19,20]. Another popular viscoplastic model, G'Sell and Jonas, was mainly designed for modeling the mechanical behavior of solid semi-crystalline polymers where the authors studied the plastic behavior of poly(vinyl chloride) and high density polyethylene[21]. Consequently, many studies were inspired by this model to describe the behavior of different polymers such as as PMMA, HDPE, PP, HIPS[22–25]. The numerical work of Atmani et al.[9] consisted in modeling the thermoforming of a HIPS yogurt container by an elasto-viscoplastic model based on G'Sell and Jonas. Morover, the latter gave acceptable results describing the mechanical behavior of fiber reinforced polymers. In the work of Schossig et al.[4], the strain rate dependent behavior of glass fiber reinforced polypropylene and polybutene-1 was experimentally investigated and modeled using the phenomenological G'Sell and Jonas law. Concerning the mechanical characterization techniques, conventional uniaxial tests are widely applied to identify the mechanical behavior of fiber reinforced thermoset polymers such as epoxy. Less frequently, biaxial testing methods have also been employed with different types of specimen including cruciform shaped samples[26–30]. In this paper, the mechanical behavior of glass fiber reinforced polypropylene (40% GF/PP) is investigated. The combined effect of strain rate and temperature is considered. Normally, in the majority of the published studies related to the mechanical characterization fiber reinforced polymers, the effect of temperature is monitored at one strain rate (mainly quasi-static) and the strain sensitivity analysis is performed at room temperature. Therefore, three strain rates and three temperatures are considered in this study. For each temperature, uniaxial tensile tests are conducted for three strain rates. The anisotropic behavior is examined as well. Additional tests are performed using uniaxial specimens extracted at different orientations to examine the anisotropy of the material. A phenomenological constitutive model, inspired by G'Sell and Jonas model[21,31], originally designed for unreinforced semi-crystalline polymers is proposed. A modification is applied to the original equation for a better description of the behavior experimentally observed. The proposed law is then numerically validated by finite element simulations of the uniaxial tensile test on the commercial software Abaqus. In the last part of this paper, the model identified from uniaxial tests is used to simulate an equi-biaxial tensile test where the state of loading is supposed to be close to that encountered during the forming process of the material. The results presented in this article lay the groundwork for a more advanced characterization technique based on biaxial tensile tests on cruciform shaped specimens. The key purpose behind this investigation is to model the complex behavior of glass fiber reinforced polypropylene during heat assisted incremental sheet forming.

Material and experimental testing

Material

The composite material used in this work is a 40% glass fiber reinforced polypropylene thermoplastic (40%GF/PP). Injection molded rectangular plates, of dimension 510x300x2 mm^3, are supplied by SABIC company (Stamax, 40YM240). Specimens for uniaxial tests are extracted by means of water-jet cutting machine in the 0°, 90° and 45° directions, where the 0° direction represents

the length of the plate. Figure 1 shows the dimensions of the uniaxial tensile specimen made of 40%GF/PP.

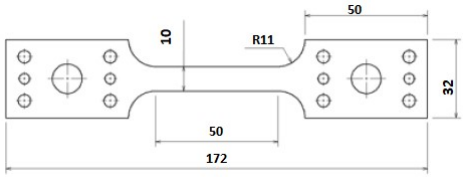

Figure 1. Dimensions of uniaxial tensile specimen (in mm).

Uniaxial Tensile tests

Uniaxial tensile tests are performed on a hydraulic machine[32] equipped with a heating system. In this work, load velocities of 0.5, 50 and 500 mm/s are tested, corresponding to initial strain rate values of 0.001, 1 and 10 s^{-1}, respectively. Experiments are carried out at three different temperatures: 20°C, 70°C and 120°C. The room temperature RT (20°C) is a conventional temperature of reference to test. Also, polypropylene is known to have a maximum continuous service temperature between 100°C and 130°C. For this reason, a temperature of 120°C is selected in this range of maximum continuous operating temperature. An intermediate temperature of 70°C is also tested. The temperature and strain rate ranges for the characterization are then directly linked to the conditions of heat forming processes.

The experimental forces are measured by a load sensor mounted on the upper fixed crosshead. Digital Image Correlation (DIC) is applied for strain measurements. This approach is nowadays extensively applied to obtain displacement and strain fields from images of a loaded part. It is applicable not only for metals, but also for polymers such as polymethyl methacrylate (PMMA)[33,34] as well as for fiber reinforced polymers e.g., Basalt fiber reinforced polypropylene and glass fiber reinforced polypropylene[11,19]. To perform DIC in this work, a speckle pattern (gray scale) is applied to the surface of the object (a white layer is first applied and then sprayed with random black dots). A high-speed/resolution camera (PHOTRON FASTCAM NOVA S9) is fixed above the specimen along with a proper lighting system ensuring that no surface heating is caused by the light. GOM Correlate software was used for the correlation procedure. Relying on A DIC guideline[35], a facet size of 21 pixels and a point distance of 7 pixels (0.12mm/pixel) are applied. A virtual extensometer is employed to calculate the length change in the region of interest, i.e. calculating the average deformation of the specimen's gauge length as illustrated in Figure 2. The use of the virtual extensometer to calculate the average deformation makes the results less sensitive to the correlation parameters. The tensile properties including Young's modulus E, ultimate tensile strength σ_{ult} and strain at failure ε_f are determined based on the Standard ISO-527 for plastics[36]. In the following tests, the effect of specimen orientation, strain rate and temperature are studied. It's important to state that the repeatability of the results is verified with three tests for each condition. An example is illustrated in Figure 3 showing the repeatability of the stress strain curves resulting from three tests performed at

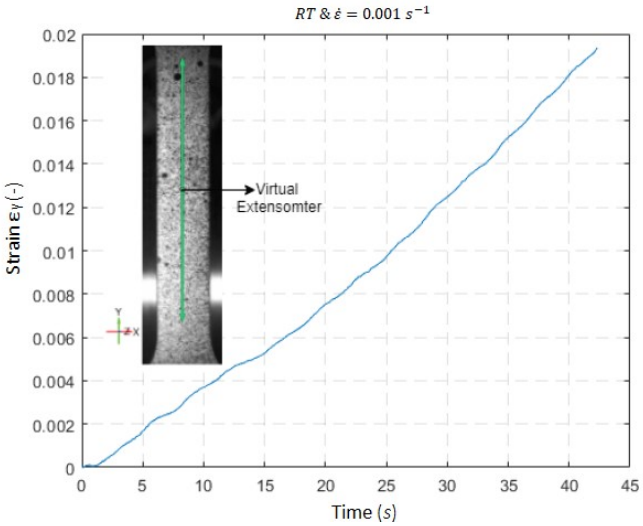

Figure 2. Strain measurement using virtual extensometer in DIC Correlate for the uniaxial tensile test at RT and 0.001 s^{-1}.

the same experimental conditions at RT and quasi-static strain rate (0.001 s^{-1}). The error bars represent the standard deviation calculated from the three tests. Good repeatability is achieved for all tested conditions.

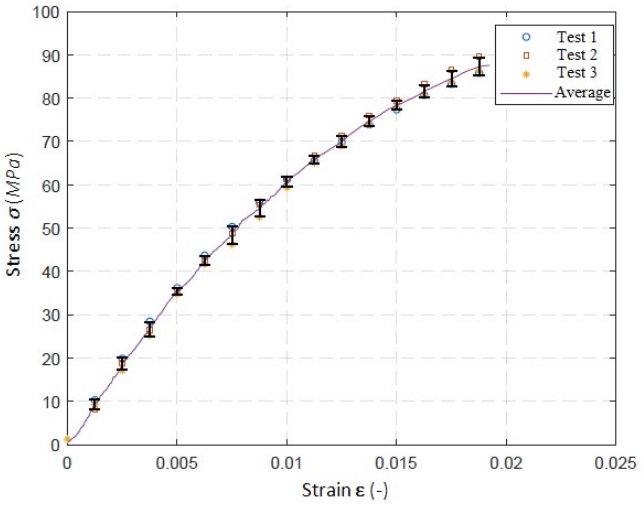

Figure 3. Repeatability test conducted at RT and 0.001s^{-1}.

Effect of specimen orientation

In order to investigate the effect of the material orientation and examine the anisotropic behavior of the material, uniaxial tensile tests are conducted at RT and quasi-static strain rate of 0.001 s^{-1}, using specimens extracted from three different orientations: i) along the length of the plate (0° orientation), ii) along the width (90° orientation) and iii) with an angle of 45°. Figure 4 gives the stress-strain curves for the three directions showing a clear difference in the material behavior. The lowest value of the stiffness is attributed to the 90° direction. The stiffness at 45° is represented by the curve located between the 0° and 90° direction curves. Moreover, the ultimate tensile strength decreases with the increase of the specimen orientation angle. The highest value of 91 MPa is reached for the 0° direction. On the other hand, the elongation at failure shows

a slight increase when the angle increases; it reaches a value of 2.3% for the 90° direction. This behavior is thought to be related to the manufacturing of the structure and the induced fibers orientation/distribution, given that the plates are rectangular and the injection port is located in the middle. The discontinuous fibers are more likely to be oriented along the longitudinal direction at the expense of the other. In this case, it is along the length of the plate (0° direction). Table 1 lists the values of obtained tensile properties for the three orientations at room temperature.

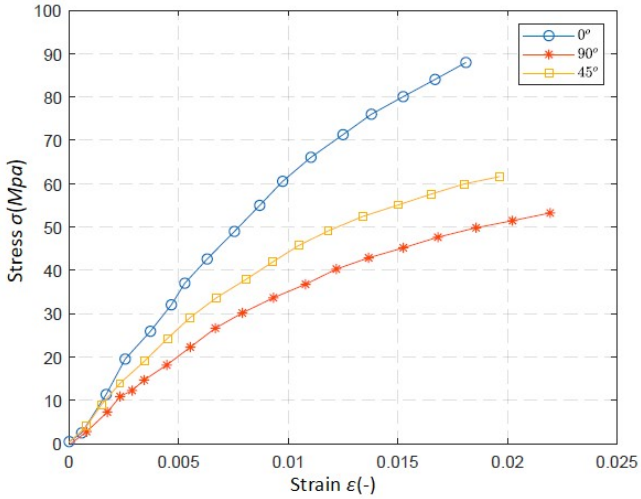

Figure 4. Uniaxial stress-strain curves at room temperature and quasi-static strain rate for three different orientations.

Table 1. Tensile properties for three different material orientations at RT.

$\theta(^\circ)$	E (MPa)	σ_{ult} (MPa)	ε_f (%)
0	7428	91	1.94
90	4122	52	2.3
45	5686	64	2.09

Effect of strain rate

To study the effect of strain rate on the mechanical behavior, test specimens extracted from the 0° direction are considered. The influence of the strain rate is clearly shown in Figure 5 where stress-strain curves are plotted for three different temperatures (20°C, Figure 5a; 70°C, Figure 5b; 120°C, Figure 5c). Note that the stress-strain behavior of the material exhibits a limited linear behavior at the beginning followed by a non-linear response.

For each temperature, three different strain rates are tested: 0.001, 1, and 10 s^{-1}. As a result, a positive strain rate effect is observed. This is remarkable for the three applied temperatures. Looking at Figure 5a, it is clear that when considering $0.001s^{-1}$ as a reference strain rate, σ_{ult} increases by 16% and 43% when the reference strain rate is multiplied by a factor of 10^3 and 10^4, respectively. The resultant maximum stress is then 130 MPa while the stress corresponding to a strain rate of $0.001s^{-1}$ is 91 MPa. In the considered strain rate range, the strain at failure and the stiffness vary slightly. Indeed, compared to the lowest strain rate, a small increase of 7% and 14% is noticed for the elongation at failure ε_f and Young's modulus E, respectively, at the highest strain rate.

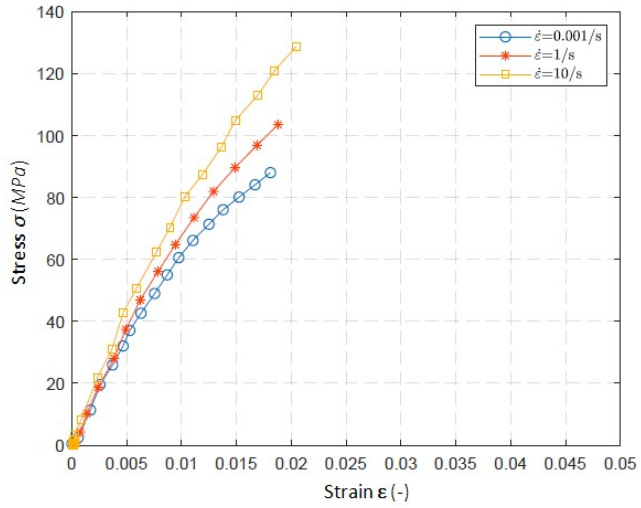

(a) T=20°C

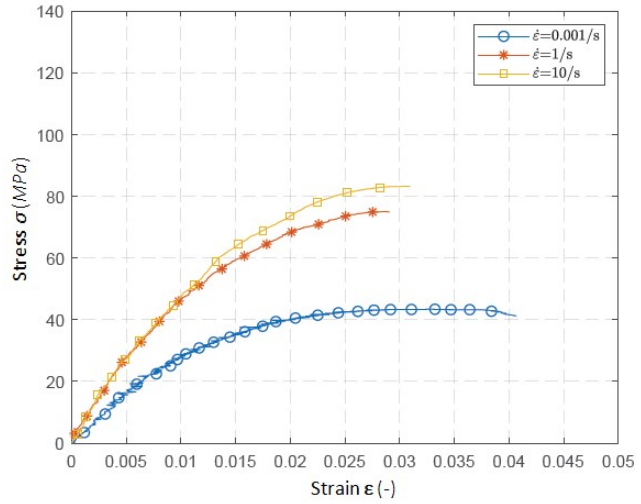

(b) T = 70°C

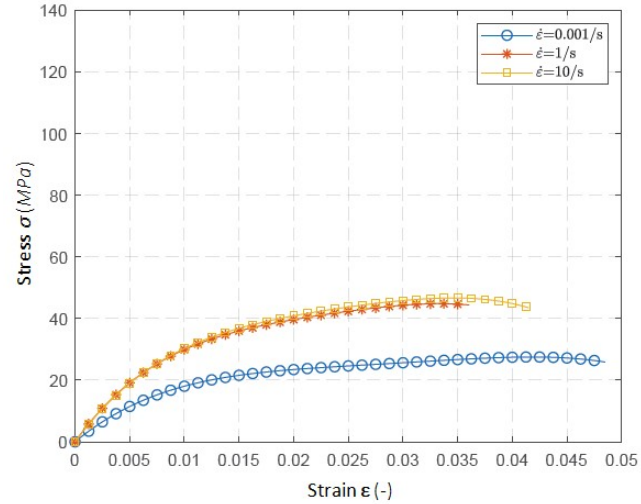

(c) T = 120°C

Figure 5. Effect of testing velocity on the behavior for three different temperatures.

For temperatures T = 70°C and T = 120°C, Figure 5b and Figure 5c respectively, the strength and the stiffness also increase with the strain rate. However, despite the clear

difference between the curves corresponding to strain rates of 0.001 and 1 s^{-1}, the curves obtained at 1 and 10 s^{-1} are relatively close. This shows that the sensitivity of the tested reinforced thermoplastic material to the strain rate becomes low at high temperatures. Note that for a strain rate of $0.001s^{-1}$, elongation at failure increases from 2% to 4.06% and 4.85% for T = 20°C, T = 70°C and T = 120°C, respectively.

Effect of temperature

The thermoplastic materials can be molded as often as desired by cooling and reheating, as long as the material is not overheated. Consequently, it is important to study the effect of temperature on the mechanical behavior of the tested material. The uniaxial tests already performed in the previous section are presented in this section as a function of the temperature. For every strain rate, three stress-strain curves corresponding to the three tested temperatures (20°C, 70°C and 120°C) are plotted in Figure 6.

Figure 6a, Figure 6b and Figure 6c show the stress-strain curves corresponding to strain rates of 0.001, 1 and 10 s^{-1}, respectively. According to these curves, the effect of temperature is noteworthy. For a quasi-static uniaxial test ($\dot{\varepsilon} = 0.001s^{-1}$), the ultimate strength decreases from 91 to 25 MPa while the elongation at failure increases from 1.94% to 4.85%. Moreover, when increasing the temperature, the stiffness decreases, for the three tested strain rates.

Figure 7 shows the combined effect of temperature and strain rate on the tensile properties of the thermoplastic material for the 0° direction.

Table 2 summarizes the different values of the tensile properties as a function of the velocity for the three tested temperatures such as the ultimate stress, the elongation at failure and Young's modulus which is defined as the slope of stress-strain curves in the deformation range 0.05%-0.25% according to ISO 527[36] .

Table 2. Effect of strain rate on the tensile properties at three different temperatures.

$\dot{\varepsilon}(s^{-1})$	E(MPa)	σ_{ult} (MPa)	ε_f (%)
$T = 20°C$			
0.001	7428	91	1.94
1	8140	107	1.96
10	9188	130	2.08
$T = 70°C$			
0.001	3454	41	4.06
1	5507	75	2.9
10	5946	84	3.09
$T = 120°C$			
0.001	2515	25	4.85
1	4215	45	3.6
10	4166	43.5	4.17

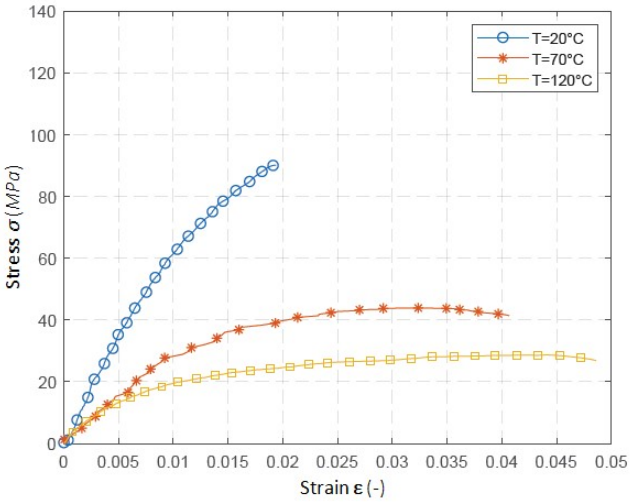

(a) $\dot{\varepsilon} = 0.001s^{-1}$

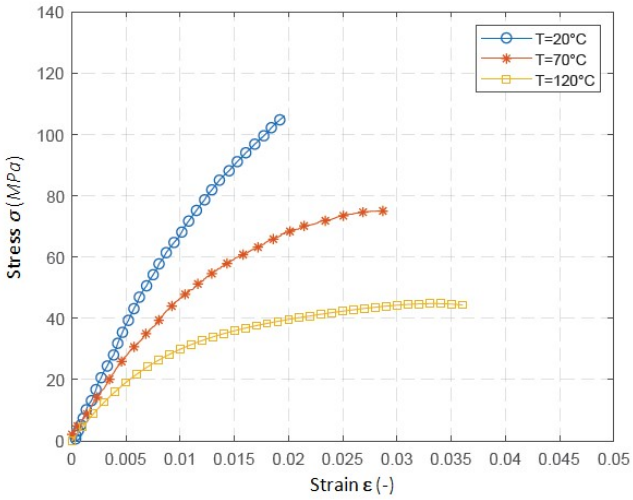

(b) $\dot{\varepsilon} = 1s^{-1}$

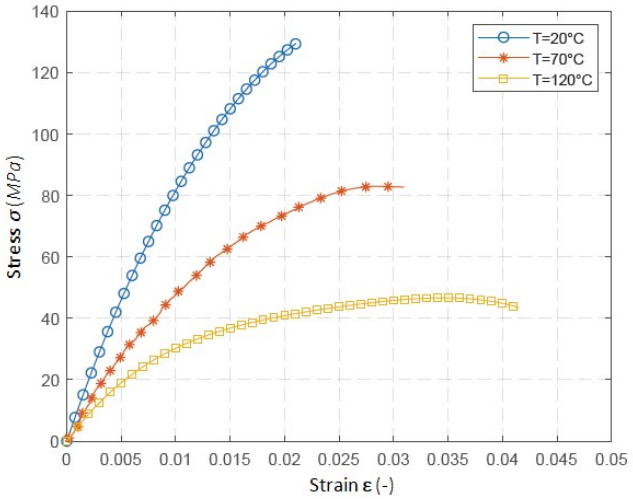

(c) $\dot{\varepsilon} = 10s^{-1}$

Figure 6. Effect of temperature on the behavior for three different strain rates.

Identification of thermomechanical model

Isotropic model

The experimental investigations performed in this work underlined the significant effect of strain rate and temperature on the mechanical behavior of discontinuous glass fiber reinforced polypropylene. In this section, the isotropic phenomenological constitutive model of G'Sell and Jonas[21,31] is selected to describe the behavior of the studied material. This model was originally designed to describe the behavior of semi-crystalline polymers. In this

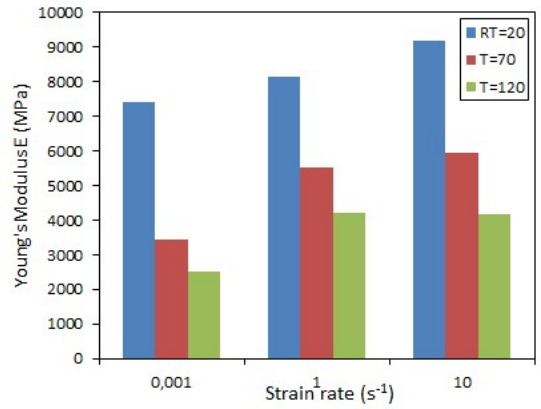

(a) Young's modulus E

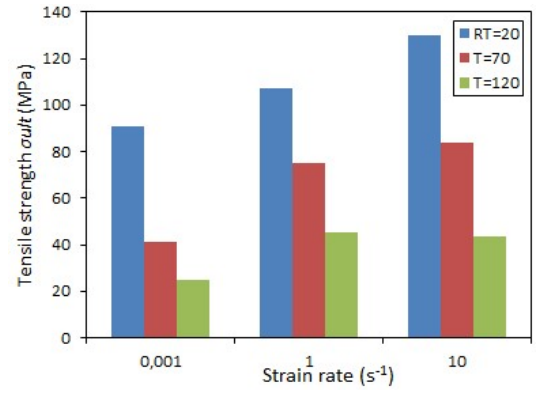

(b) Ultimate strength σ_{ult}

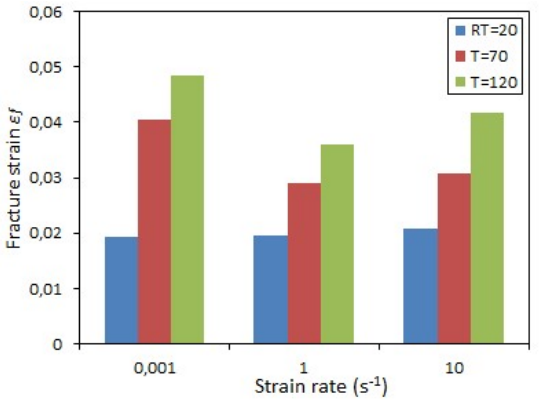

(c) Strain at failure ε_f

Figure 7. Effect of temperature and strain rate on the tensile properties for the longitudinal orientation.

work, a modification of the constitutive equation is proposed for a better description of the observed experimental behavior. The material parameters of the model are initially calibrated based on the uniaxial tensile test results performed on specimens along the 0° orientation. The anisotropy is integrated, in the following section, once the model is validated for the longitudinal direction. The original constitutive equation of the model is stated in equation 1:

$$\sigma(\varepsilon,\dot{\varepsilon}) = K \cdot \exp\left(h\varepsilon^2\right) \cdot (1-\exp(-W\varepsilon)) \cdot \dot{\varepsilon}^m \qquad (1)$$

Where:

- σ is the equivalent stress in MPa,
- ε is the equivalent strain,
- $\dot{\varepsilon}$ is the equivalent strain rate,
- m is the strain rate sensitivity,
- K is a scaling factor in MPa,
- h and W are material parameters.

Behavior at low strain levels is represented by the term $(1-\exp(-W\varepsilon))$. The term $\exp\left(h\varepsilon^2\right)$ represents the stiffening of the material at large deformations[9] which is neglected (h = 0) in this work due to the low level of deformation at failure observed from the experimental results. Additionally, the effect of the temperature can be incorporated in the model equation by performing a temperature sensitivity analysis for the material parameters and expressing them as a function of temperature. Therefore, the constitutive equation considered in this work becomes (equation 2):

$$\sigma(\varepsilon,\dot{\varepsilon},T) = K(T) \cdot (1-\exp(-W(T)\cdot\varepsilon)) \cdot \dot{\varepsilon}^{m(T)} \qquad (2)$$

As proposed in many studies[9,22–25], the equation of the model can be modified to clearly identify the linear and non-linear behaviors. Consequently, in this work, the constitutive equation of the model is modified as stated in equation 3:

$$\begin{cases} \sigma = E(\dot{\varepsilon},T)\cdot\varepsilon & \text{for } \sigma < \sigma_y \\ \sigma = \sigma_y(\dot{\varepsilon},T) & \\ \quad +K(T)\cdot(1-\exp(-W(T).\varepsilon_p))\,\dot{\varepsilon}^{m(T)} & \text{for } \sigma > \sigma_y \end{cases} \qquad (3)$$

The equivalent deformation and equivalent plastic deformation are represented by ε and ε_p, respectively. The latter is determined from the experimental stress-strain curves based on equation 4:

$$\varepsilon_p = \varepsilon - \frac{\sigma}{E} \qquad (4)$$

Accordingly, the yield strength σ_y is identified as the stress level at which plastic deformation initiates, indicating that ε_p exceeds zero. The strain rate sensitivity m is determined in the non-linear region (equation 5) as the slope of the plot $\ln(\sigma-\sigma_y(\dot{\varepsilon},T))$ vs. $\ln\dot{\varepsilon}$, at a given temperature T and a plastic strain level ε_p, as stated in equation (6). The value of m is assumed to be constant for all strain levels; an average of m values is then taken at five different strain levels, as suggested by[21]:

$$\sigma-\sigma_y(\dot{\varepsilon},T) = K(T)\,(1-\exp(-W(T).\varepsilon_p))\,\dot{\varepsilon}^m \qquad (5)$$

$$m = \left.\frac{\partial\ln(\sigma-\sigma_y(\dot{\varepsilon},T))}{\partial\ln\dot{\varepsilon}}\right|_{\varepsilon_p,T} \qquad (6)$$

The parameters K and W are analytically determined by parameter regression using a nonlinear optimization function in MATLAB. The cost function to be minimized is defined by the error δ as follows,

$$\delta = \min\sum_{i=1}^{n}\left(\sigma_{\text{model}} - \sigma_{\text{experimental}}\right)^2 \qquad (7)$$

Where n is the total number of data points, σ_{model} is the predicted stress, and $\sigma_{experimental}$ is the stress calculated from the force measured experimentally.

To generalize equation 3, Young's modulus E and yield strength σ_y are approximated by the following relations,

$$E(T,\dot{\varepsilon}) = E_0(T)\dot{\varepsilon}^m \tag{8}$$

$$\sigma_y(T,\dot{\varepsilon}) = \sigma_0(T)\dot{\varepsilon}^m \tag{9}$$

The parameters of G'Sell and Jonas model identified for each temperature are summarized in Table 3.

Table 3. Material parameters determined for the three different temperatures.

$T(°C)$	$m(-)$	$K(MPa)$	$W(-)$	$\sigma_0(MPa)$	$E_0(MPa)$
20	0.0347	80	419.5	34.96	8621
70	0.074	51.3	290.7	19.9	5387
120	0.07	27.3	212.9	13.2	3827

Anisotropy modeling

It is clear from the stress-strain curves at 0°, 45° and 90° that the anisotropy in this material cannot be neglected. As suggested by some authors[37–42], the equivalent stress $\psi(\sigma)$ can be described by the conventional Hill 48 yield criterion[43] (equation 10):

$$\psi(\sigma) = \sqrt{\begin{array}{c} F(\sigma_{22}-\sigma_{33})^2 + G(\sigma_{33}-\sigma_{11})^2 \\ +H(\sigma_{11}-\sigma_{22})^2 + 2(L\sigma_{23}^2 + M\sigma_{13}^2 + N\sigma_{12}^2) \end{array}} \tag{10}$$

In the case of plane stress the equation reduces to:

$$\psi(\sigma) = \sqrt{\begin{array}{c} (G+H){\sigma_{11}}^2 + (H+F){\sigma_{22}}^2 \\ -2H\sigma_{11}\sigma_{22} + 2N{\sigma_{12}}^2 \end{array}} \tag{11}$$

The parameters F, G, H, and N are determined from the yield stress ratio $R(\theta)$ at a given orientation θ with respect to the 0° direction (equation 12):

$$R(\theta) = \frac{1}{\sqrt{\begin{array}{c} F\cdot\sin^2\theta + G\cdot\cos^2\theta + H + \\ (2N-F-G-4H)\sin^2\theta\cos^2\theta \end{array}}} = \frac{\sigma_y(\theta)}{\sigma_y(0°)} \tag{12}$$

The plastic potentials in ABAQUS are defined as:

$$\begin{array}{c} R_{11} = \sqrt{\frac{1}{G+H}}, R_{22} = \sqrt{\frac{1}{F+H}}, \\ R_{33} = \sqrt{\frac{1}{G+F}}, R_{12} = \sqrt{\frac{3}{2N}}, R_{13} = R_{23} = 1 \end{array} \tag{13}$$

Table 4 shows the Hill's parameters representing the anisotropy of the studied material at RT and quasi-static strain rate. The same parameters are applied for all the tested conditions.

Table 4. Parameters of Hill's plasticity for anisotropy.

Direction $\theta(°)$	Yield stress $\sigma_y(MPa)$	Yield stress ratio R(θ)	Hill coefficients	Plastic potentials
0°	29.37	1	F = 2.7	$R_{11} = 1$
90°	16.48	0.56	G = 0.53	$R_{22} = 0.56$
45°	20.78	0.707	H = 0.47	$R_{33} = 0.6$
			N = 2.38	$R_{12} = 0.79$
				$R_{13} = R_{23} = 1$

Results and Discussions

Numerical validation of the identified model

By applying the same uniaxial experimental conditions (homogeneous temperature and velocity), the calibrated model is numerically validated by performing finite element simulations of the uniaxial tensile tests on the commercial FE software ABAQUS. The model is implemented by FORTRAN code as a user subroutine UHARD. Only the gauge region of the specimen is modeled. Due to the homogeneous strain field, the model is not sensitive to the element size, number and type. Figure 8 shows the stress-strain variations obtained experimentally for 0° orientation when compared with the simulation results. As shown in the figures, the experimental and numerical results are in good agreement. The mean relative error between experimental and simulation stress-strain curves is indicated in the figures.

On the other hand, the anisotropy is numerically validated by performing finite element simulation using Hill's yield criterion while integrating the parameters determined in the previous section. The three directions (0°, 45° and 90°) are then numerically simulated and compared to the uniaxial experimental results, in Figure 9. It shows that Hill's anisotropic criterion associated to the identified numerical model agrees well with the uniaxial experimental results.

Numerical validation of the identified model using biaxial results

As already discussed, for the future work, the identified phenomenological model will be used to simulate the forming of a plate made of 40% GF/PP, through the heat assisted incremental sheet forming process. The in-plane biaxial tensile test on cruciform specimens is a promising characterization tool in which the material can be loaded from shear to expansion, according to strain states similar to those encountered in forming processes. Therefore, it is worth checking the ability of the model identified from the uniaxial tensile tests to successfully model biaxial stress states such as those encountered by the material during the envisaged forming process. In the following section, a biaxial testing setup used to perform an in-plane equi-biaxial tensile test on a 40%GF/PP thermoplastic cruciform specimen at room temperature and quasi-static condition is briefly presented. Then, experimental results are compared with numerical ones using the model identified from the uniaxial characterization.

Experimental biaxial tensile tests

In-plane biaxial tensile testing on flat cruciform specimens is a promising technique to evaluate the performance of sheet metal/composite components under various loading conditions. This loading configuration is representative of the stress state that the components experience in real-world applications[30,44]. In the frame of the biaxial tests, Liu et al.[45] proposed a cruciform specimen to identify the hardening behavior of metallic sheets subjected to large deformations. As a first approach, this optimized shape of the cruciform specimen is considered in this study. Figure 10a shows the used cruciform specimen with its dimensions in Figure 10b. The specimens are machined from the same plates used for the uniaxial tests. From a 2mm initial thickness, a thinning

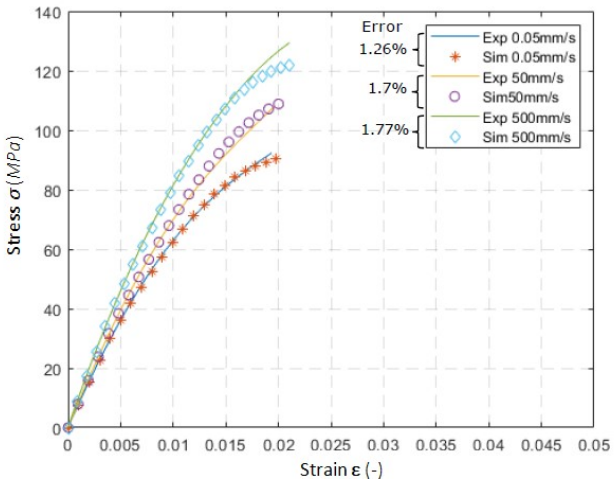

(a) T = 20°C

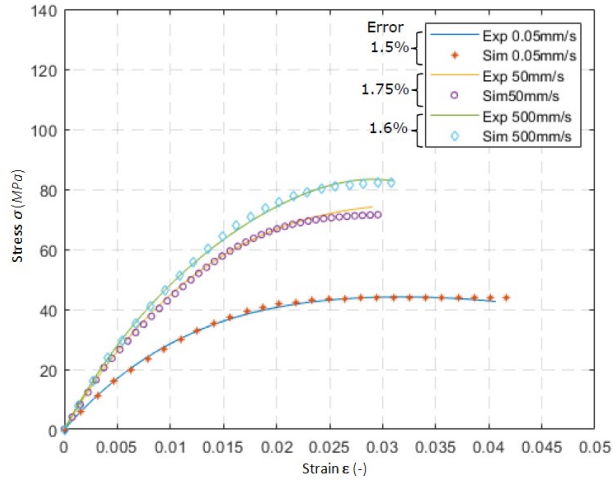

(b) T = 70°C

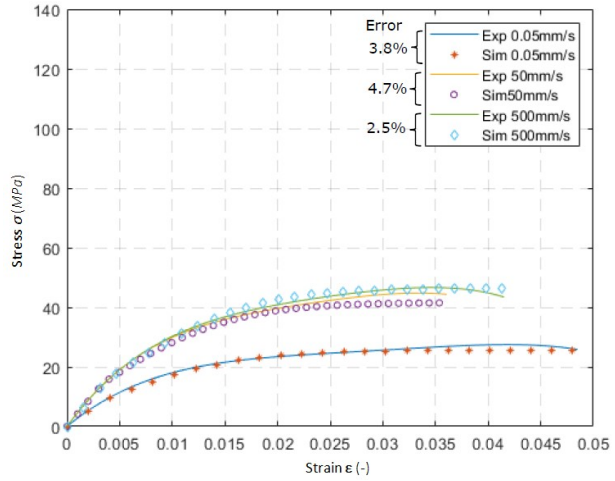

(c) T = 120°C

Figure 8. Comparison between experimental and numerical simulation of stress-strain curves at three different temperatures for 0° orientation. The mean relative error between the experimental and simulation curves is also indicated.

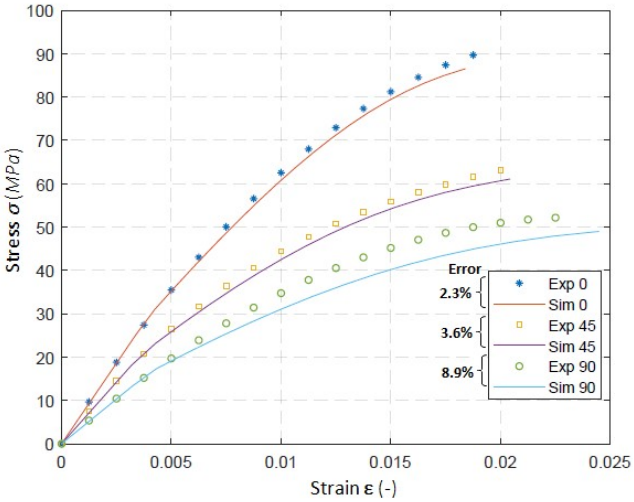

Figure 9. Comparison between experimental and simulation results for the three orientations 0°, 45° and 90° taking into account the anisotropy (Hill's criterion) of the material along with the mean square error percentage.

(a) Biaxial tensile test cruciform specimen designed by Liu et al.[45,46].

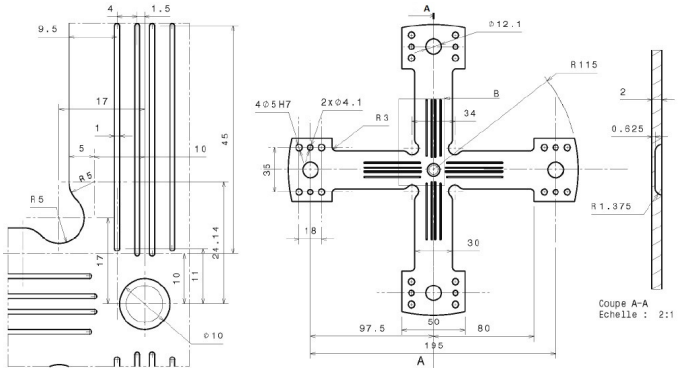

(b) Dimensions of the cruciform specimen (in mm).

Figure 10. Cruciform specimen used for biaxial tensile testing

of the central zone is made (up to a final thickness of 0.625 mm) to ensure failure in this zone.

A servo-hydraulic biaxial tensile machine[26], with four independent actuators, is used to conduct the biaxial tensile tests. The force is measured on each axis of the machine using gauge sensors. To measure the strain, the same digital image correlation technique (DIC), presented in the uniaxial tests, is used. The high speed camera is placed above the central zone of the specimen. The equi-biaxial tensile test is performed at room temperature and at a tensile speed of 0.1mm/s imposed on each specimen arm. This loading induces an average equivalent strain rate in the central zone of approximately $0.003s^{-1}$ which is close to the strain rate range obtained from the uniaxial tensile test realized at RT

and for quasi-static condition. Figure 11 shows the force and the strain curves resulting from the biaxial tensile test. As shown in the figure, maximum forces of Fx = 1400 N and Fy = 1100 N are obtained at failure where x-axis is along the length of the plate i.e, 0° and y-axis is the width of plate i.e, 90°, respectively. The difference between the forces is due to the anisotropy of the tested material. Also, the obtained maximum strains at failure are $\varepsilon_{f,x}$ = 1% and $\varepsilon_{f,y}$ = 2%, corresponding for x-axis and y-axis, respectively. The equivalent Von-Mises strain ε_{Mises} is found to have a maximum value of 3.1% at failure. This value is relatively higher than the deformation at failure attained during the uniaxial tensile test (strain of 2%) for the same experimental conditions.

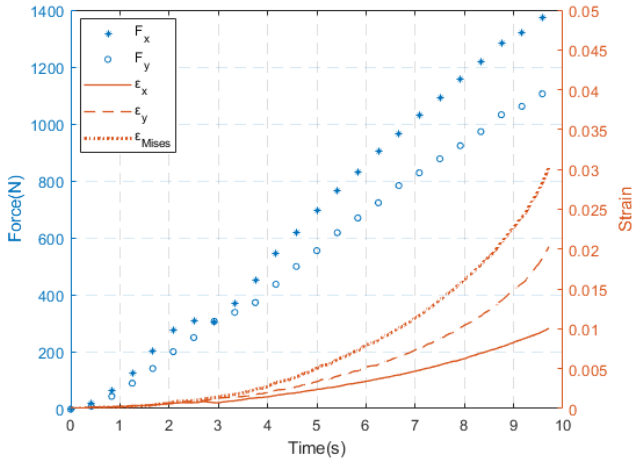

Figure 11. Force and strain curves for biaxial tensile test at room temperature and for a tensile test velocity of 0.1mm/s imposed on each specimen arm.

Simulation of biaxial tensile tests

The validity of the phenomenological model identified from the uniaxial characterization is evaluated by the FE simulation of the experimentally performed in-plane equi-biaxial tensile test. The material parameters outlined in Table 3 along with Hill's anisotropic potentials summarized in Table 4 are used to simulate the biaxial tensile test. As a first step, the test conducted at RT and quasi-static velocity is simulated. Due to the symmetry, only a quarter of the cruciform specimen is considered. Therefore, on each arm, half of the experimentally obtained forces are applied i.e. Fx/2 along x-axis and Fy/2 along y-axis. More details concerning the FE simulation of the biaxial test simulations are given in the work of Liu et al.[45,46]. A comparison between the experimental and numerical equivalent Mises strain curves is shown in Figure 12. It is clearly obvious that simulating the biaxial test using the parameters identified from the uniaxial tests leads to poor agreement between experimental and numerical results. This discrepancy shows that the behavior of the material under biaxial loadings must be integrated in the calibration stage of the material model. Therefore, an inverse analysis based on the in-plane biaxial test is required for the re-identification of the model's parameters.

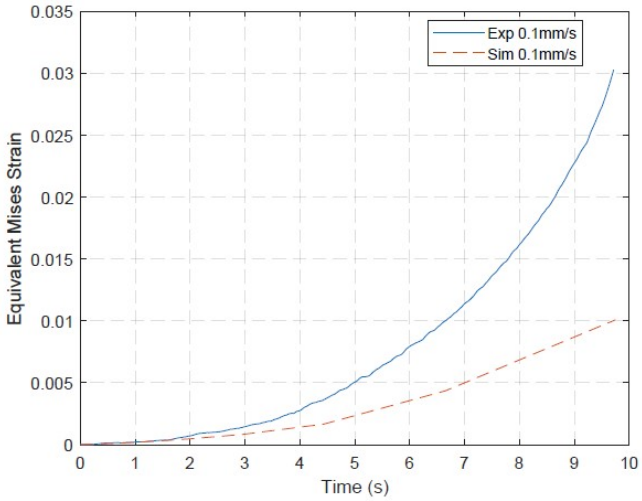

Figure 12. Comparing the experimental equivalent Mises strain with the numerical equivalent Mises strain simulated based on the material parameters identified from the uniaxial characterization.

Conclusion

The mechanical behavior of glass fiber reinforced polypropylene is investigated, focusing on the combined effect of strain rate/temperature on the material response. A series of uniaxial tensile tests are performed at room temperature up to 120°C, for strain rates ranging from quasi-static conditions to 10 s^{-1}. As suspected, tensile properties are very sensitive to temperature and strain rate. A phenomenological constitutive behavior law inspired by the G'Sell and Jonas model is identified. The original equation is modified according to the experimental observations of the uniaxial characterization. The model parameters are calibrated from the uniaxial results. Moreover, in order to take into account the anisotropy, the effect of the material orientation is examined by performing uniaxial tests at 0°, 45° and 90° with respect to the length of the plate. The influence of the orientation is detectable on the stress-strain evolutions and tensile properties. Consequently, the results are utilized to calibrate the parameters of Hill's criterion. The model is then implemented in Abaqus to simulate the uniaxial tensile tests and good agreement is shown between experimental and numerical results. The validity of the identified model should be inspected when the material is subjected to a biaxial stress state as is the case during heat assisted forming. Therefore, as an introduction to future tasks, an equi-biaxial tensile test on a dedicated cruciform specimen is simulated at room temperature and quasi-static strain rate conditions using the identified uniaxial model. Numerical results are compared to the experimental ones showing that the predicted model does not fit with the actual biaxial behavior. This proves the importance of integrating the biaxial characterization in the model identification procedure. In future work, the material parameters of G'Sell and Jonas model will be re-calibrated based on both uniaxial and biaxial tensile tests for temperatures and strain rates corresponding to the conditions experienced by the material during its forming stage.

Conflict of Interest

None declared.

Acknowledgments

This project has been funded by "Region Bretagne" of France. It was also supported by the Lebanese University. The authors also acknowledge "SABIC" company for providing the tested material.

References

1. Tanasa, F. & Zanoaga, M. Fiber-reinforced polymer composites as structural materials for aeronautics. Proceedings Of The International Conference Of Scientific Paper, Brasov, 23–25 May 2013. (2013)
2. Verma, D., Gope, P., Shandilya, A., Gupta, A., Maheshwari, M. & Others Coir fibre reinforcement and application in polymer composites. J. Mater. Environ. Sci. **4**, 263-276 (2013)
3. Stewart, R. Thermoplastic composites—recyclable and fast to process. Reinforced Plastics. **55**, 22-28 (2011)
4. Schoßig, M., Bierögel, C., Grellmann, W. & Mecklenburg, T. Mechanical behavior of glass-fiber reinforced thermoplastic materials under high strain rates. Polymer Testing. **27**, 893-900 (2008)
5. Greco, A., Gennaro, R. & Maffezzoli, A. Thermoforming of thermoplastics matrix composites. Wiley Encyclopedia Of Composites. pp. 1-15 (2011)
6. Zhao, F., Guo, W., Li, W., Mao, H., Yan, H. & Deng, J. A Study on Hot Stamping Formability of Continuous Glass Fiber Reinforced Thermoplastic Composites. Polymers. **14**, 4935 (2022)
7. Zhu, H., Ou, H. & Popov, A. Incremental sheet forming of thermoplastics: a review. The International Journal Of Advanced Manufacturing Technology. **111**, 565-587 (2020)
8. Nasraoui, M., Forquin, P., Siad, L. & Rusinek, A. Influence of strain rate, temperature and adiabatic heating on the mechanical behaviour of poly-methyl-methacrylate: experimental and modelling analyses. Materials & Design. **37** pp. 500-509 (2012)
9. Atmani, O., Abbès, F., Li, Y., Batkam, S. & Abbès, B. Experimental investigation and constitutive modelling of the deformation behaviour of high impact polystyrene for plug-assisted thermoforming. Mechanics & Industry. **21**, 607 (2020)
10. Wang, Z., Zhou, Y. & Mallick, P. Effects of temperature and strain rate on the tensile behavior of short fiber reinforced polyamide-6. Polymer Composites. **23**, 858-871 (2002)
11. Duan, S., Mo, F., Yang, X., Tao, Y., Wu, D. & Peng, Y. Experimental and numerical investigations of strain rate effects on mechanical properties of LGFRP composite. Composites Part B: Engineering. **88** pp. 101-107 (2016)
12. Cui, J., Wang, S., Wang, S., Li, G., Wang, P. & Liang, C. The effects of strain rates on mechanical properties and failure behavior of long glass fiber reinforced thermoplastic composites. Polymers. **11**, 2019 (2019)
13. Basrani, J., Kumar, M. & Kumar, P. An Experimental Study of Static and Dynamic Behavior of the Hybrid Composite. Journal Of Natural Fibers. **19**, 15475-15487 (2022)
14. Kumar, N. & Rao, V. Hyperelastic Mooney-Rivlin model: determination and physical interpretation of material constants. Parameters. **2**, 01 (2016)
15. Gong, Y., Peng, X., Yao, Y. & Guo, Z. An anisotropic hyperelastic constitutive model for thermoplastic woven composite prepregs. Composites Science And Technology. **128** pp. 17-24 (2016)
16. Pham, X., Thibault, F. & Lim, L. Modeling and simulation of stretch blow molding of polyethylene terephthalate. Polymer Engineering & Science. **44**, 1460-1472 (2004)
17. Guzman-Maldonado, E., Hamila, N., Boisse, P. & Bikard, J. Thermomechanical analysis, modelling and simulation of the forming of pre-impregnated thermoplastics composites. Composites Part A: Applied Science And Manufacturing. **78** pp. 211-222 (2015)
18. Peng, X., Yin, H., Chen, J. & Liu, X. A phenomenological thermal-mechanical viscoelastic constitutive modeling for polypropylene wood composites. Advances In Materials Science And Engineering. **2012** (2012)
19. Wang, S., Yao, Y., Tang, C., Li, G. & Cui, J. Mechanical characteristics, constitutive models and fracture behaviors of short basalt fiber reinforced thermoplastic composites under varying strain rates. Composites Part B: Engineering. **218** pp. 108933 (2021)
20. Chen, X., Li, Y., Zhi, Z., Guo, Y. & Ouyang, N. The compressive and tensile behavior of a 0/90 C fiber woven composite at high strain rates. Carbon. **61** pp. 97-104 (2013)
21. G'sell, C. & Jonas, J. Determination of the plastic behaviour of solid polymers at constant true strain rate. Journal Of Materials Science. **14**, 583-591 (1979)
22. Atmani, O., Abbès, B., Abbès, F., Li, Y. & Batkam, S. Identification of a thermo-elasto-viscoplastic behavior law for the simulation of thermoforming of high impact polystyrene. AIP Conference Proceedings. **1960**, 120003 (2018)
23. Sala, G., Di Landro, L. & Cassago, D. A numerical and experimental approach to optimise sheet stamping technologies: polymers thermoforming. Materials & Design. **23**, 21-39 (2002)
24. Abbès, B., Zaki, O. & Safa, L. Experimental and numerical study of the aging effects of sorption conditions on the mechanical behaviour of polypropylene bottles under columnar crush conditions. Polymer Testing. **29**, 902-909 (2010)
25. Abbès, F., Tran, N., Abbès, B. & Guo, Y. Modelling of the degradation of mechanical properties of high-density polyethylene based-packaging exposed to amyl acetate solution. Polymer Testing. **59** pp. 449-461 (2017)
26. Kobeissi, A., Rahme, P., Leotoing, L. & Guines, D. Strength characterization of glass/epoxy plain weave composite under different biaxial loading ratios. Journal Of Composite Materials. **54**, 2549-2563 (2020)
27. Bhatnagar, N., Bhardwaj, R., Selvakumar, P. & Brieu, M. Development of a biaxial tensile test fixture for reinforced thermoplastic composites. Polymer Testing. **26**, 154-161 (2007)
28. Kobeissi, A. Caractérisation mécanique des matériaux composites à partir d'un essai de traction biaxiale intégrant l'effet des chemins de déformation. (INSA de Rennes; Université Libanaise. Faculté de génie,2019)
29. Chen, A. & Matthews, F. A review of multiaxial/biaxial loading tests for composite materials. Composites. **24**, 395-406 (1993)
30. Hartmann, S., Gilbert, R. & Sguazzo, C. Basic studies in biaxial tensile tests. GAMM-Mitteilungen. **41**, e201800004 (2018)

31. G'sell, C., Aly-Helal, N. & Jonas, J. Effect of stress triaxiality on neck propagation during the tensile stretching of solid polymers. Journal Of Materials Science. **18**, 1731-1742 (1983)
32. Liang, J., Guines, D. & Léotoing, L. Thermo-viscoplastic behavior of AA6061 under dynamic biaxial loadings. AIP Conference Proceedings. **2113**, 180014 (2019)
33. Alavi, S., Ayatollahi, M., Daneshfar, M. & Bahrami, B. Experimental stress determination of blunt notches under combinations of modes I and II loading. Engineering Structures. **278** pp. 115517 (2023)
34. Alavi, S., Ayatollahi, M., Jamali, J. & Petru, M. On the applicability of digital image correlation method in extracting the higher order terms in stress field around blunt notches. Theoretical And Applied Fracture Mechanics. **121** pp. 103436 (2022)
35. Bigger, R., Blaysat, B., Boo, C., Grewer, M., Hu, J., Jones, A., Klein, M., Lava, P., Pankow, M., Raghavan, K., Reu, P., Schmidt, T., Siebert, T., Simonsen, M., Trim, A., Turner, D., Vieira, A. & Weikert, T. A Good Practices Guide for Digital Image Correlation. (2018)
36. Organization, I. ISO 527-1: 2019—Plastics—Determination of Tensile Properties—Part 1: General Principles. (International Standards Organization Geneva, Switzerland,2019)
37. Van Erp, T., Reynolds, C., Peijs, T., Van Dommelen, J. & Govaert, L. Prediction of yield and long-term failure of oriented polypropylene: Kinetics and anisotropy. Journal Of Polymer Science Part B: Polymer Physics. **47**, 2026-2035 (2009)
38. Abida, M., Mars, J., Gehring, F., Vivet, A. & Dammak, F. Anisotropic visco-elastoplastic modeling of quasi-unidirectional flax fiber reinforced epoxy behavior: an investigation on low-velocity impact response. Journal Of Renewable Materials. **6**, 464-476 (2018)
39. Amiri-Rad, A., Pastukhov, L., Govaert, L. & Van Dommelen, J. An anisotropic viscoelastic-viscoplastic model for short-fiber composites. Mechanics Of Materials. **137** pp. 103141 (2019)
40. Amiri-Rad, A., Wismans, M., Pastukhov, L., Govaert, L. & Dommelen, J. Constitutive modeling of injection-molded short-fiber composites: Characterization and model application. Journal Of Applied Polymer Science. **137**, 49248 (2020)
41. Joki, R., Grytten, F. & Osnes, H. Coupling of plasticity and damage in glass fibre reinforced polymer composites. EPJ Web Of Conferences. **26** pp. 04028 (2012)
42. Pastukhov, L. & Govaert, L. Plasticity-controlled failure of fibre-reinforced thermoplastics. Composites Part B: Engineering. **209** pp. 108635 (2021)
43. Hill, R. A theory of the yielding and plastic flow of anisotropic metals. Proceedings Of The Royal Society Of London. Series A. Mathematical And Physical Sciences. **193**, 281-297 (1948)
44. Chen, J., Zhang, J. & Zhao, H. Development and Experimental Verification of a High-Temperature and In-Plane Biaxial Testing Apparatus. Machines. **10**, 1054 (2022)
45. Liu, W., Guines, D., Leotoing, L. & Ragneau, E. Identification of sheet metal hardening for large strains with an in-plane biaxial tensile test and a dedicated cross specimen. International Journal Of Mechanical Sciences. **101** pp. 387-398 (2015)
46. Liu, W. Identification of strain rate dependent hardening sensitivity of metallic sheets under in-plane biaxial loading. (Rennes, INSA,2015)